Hindawi
International Journal of Aerospace Engineering
Volume 2017, Article ID 3174140, 10 pages
https://doi.org/10.1155/2017/3174140

Research Article

Experimental Study of the Swirling Oxidizer Flow in HTPB/N_2O Hybrid Rocket Motor

Mohammad Mahdi Heydari and Nooredin Ghadiri Massoom

Malek Ashtar University of Technology, Babaei Highway, Lavizan, Tehran 15875-1774, Iran

Correspondence should be addressed to Mohammad Mahdi Heydari; mmheydary@gmail.com

Received 18 April 2017; Accepted 26 July 2017; Published 27 August 2017

Academic Editor: Franco Bernelli-Zazzera

Effects of swirling oxidizer flow on the performance of a HTPB/N_2O Hybrid rocket motor were studied. A hybrid propulsion laboratory has been developed, to characterize internal ballistics characteristics of swirl flow hybrid motors and to define the operating parameters, like fuel regression rate, specific impulse, and characteristics velocity and combustion efficiency. Primitive variables, like pressure, thrust, temperature, and the oxidizer mass flow rate, were logged. A modular motor with 70 mm outer diameter and variable chamber length is designed for experimental analysis. The injector module has four tangential injectors and one axial injector. Liquid nitrous oxide (N_2O) as an oxidizer is injected at the head of combustion chamber into the motor. The feed system uses pressurized air as the pressurant. Two sets of tests have been performed. Some tests with axial and tangential oxidizer injection and a test with axial oxidizer injection were done. The test results show that the fuel grain regression rate has been improved by applying tangential oxidizer injection at the head of the motor. Besides, it was seen that combustion efficiency of motors with the swirl flow was about 10 percent more than motors with axial flow.

1. Introduction

The hybrid rocket propulsion system is one kind of chemical propulsion systems which becomes attractive today. Safety, low investment, availability, and good performance are some of its features that make it a desirable propulsion system. These characteristics are obtained by a combination of liquid propulsion system and solid propulsion system features. By this alternative, it is possible to perform a vast range of missions from low orbit missions like sounding rocket [1, 2] and target drones [3] to space missions such as transportation vehicles [4, 5], thrusters [6], and upper-stage motors [7]. In this type of propulsion system, usually, the solid fuel is a cylinder with port(s) in it, placed between injector(s) and nozzle (shown in Figure 1). Injected liquid or gas oxidizer flows through the port(s).

One important characteristic of classic hybrid motors is the low regression rate of fuel, which is mentioned as a deficiency for this type of propulsion system. Another problem in using this system is nonuniform regression of fuel in longitudinal direction. Jones et al. [8] showed that the fuel regression rate can be increased by inducing a vortex in the combustion chamber. Their study indicated an increase of 16.7% in fuel regression rate for the vortex injection over the axial injection. They used High Density Polyethylene (HDPE) as the fuel and gaseous oxygen (GOX) as the oxidizer. PP and PMMA fuel grains were burned under the swirling and nonswirling oxygen flow conditions by Masugi et al. [9]. They used a small hybrid rocket engine with a large quartz glass window to directly observe the combustion chamber from the front. They stated that, for both PP and PMMA fuels, the swirling flames were found to develop closer to the grain surface than those without swirl, resulting in an increase in the regression rates. A study on vortex injection in hybrid rocket motors with nitrous oxide as the oxidizer and paraffin as the fuel has been performed by Bellomo et al. [10]. Measured performances showed an increase in regression rate up to 51%. Yuasa et al. pushed experiments further and developed a small sounding hybrid rocket with a swirling-oxidizer-type engine [11]. They studied the combustion mechanism of a GOX/PMMA small hybrid rocket of swirling oxidizer flow and found that applying

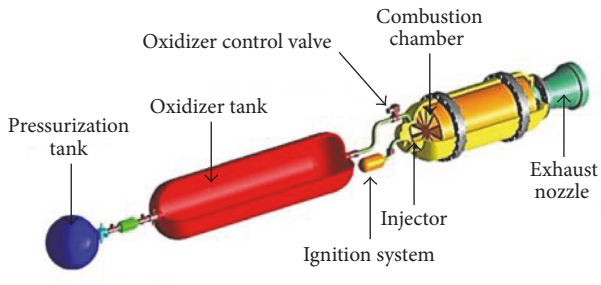

Figure 1: Classic hybrid motor.

swirl to an oxidizer flow increased fuel regression rates [12, 13]. Knuth et al. investigated the solid-fuel regression rate behavior and operating characteristics of vortex hybrid rocket engines [14]. They had tested motors with thrusts up to 960 N with gaseous oxygen and HTPB solid fuel. They measured average fuel regression rates up to seven times larger than classical hybrid motors. Kumar investigated the effect of swirl on fuel regression rate numerically. Parametric study of geometric characteristics showed that swirl is more effective for short grains ($L/D < 5$) and large diameter grains [15].

An important fuel and oxidizer composition which is used in the most famous application of hybrid motors, named Space Ship One, is HTPB/N_2O [16]. There are no studies examining oxidizer swirl flow effects on the regression rate and motor performance for this propellant composition. In the present study, this composition was used as propellant. Four tangential injectors were used to generate swirl flow in the motor. Tests have been conducted to study the effects of applying oxidizer swirl flow on this composition. The oxidizer mass flow rate was constant during tests as cavitating venturi was used.

2. Experimental Apparatus and Test Procedure

Figure 2 shows a schematic of the hybrid rocket motor laboratory. Nitrous oxide is used as oxidizer. It is pressurized by high pressure air. After test, high pressure gaseous nitrogen is used to purge the feed line and motor and to cool down motor as well. This helps to prevent undesired burning after test and provides a sharp thrust termination. Pressure transducers, thermocouples, flow meter, and load cell were used to log test data. Pressure transducers are TML PWF-PB series. A TML CLA-1KNA load cell is used to measure thrust of the motor, which is mounted on a rail and wagon mechanism. As it is shown in Figure 2, there is a T-junction in axial injection feed line, which one of its ends sits on the load cell. The load cell itself is mounted on a structure bolted to stand. Because the oxidizer inlets are perpendicular with respect to axial flow, it will not affect the measured thrust of the motor. The type K thermocouple is used to measure oxidizer temperature in the oxidizer run tank.

The oxidizer mass flow rate was measured in two ways. Both cavitating venturi and differential pressure flow meter were used in oxidizer feed line. The model of the smart differential pressure transmitter is SHHDP-9600-F12. By using a cavitating venturi in oxidizer feed line, the oxidizer mass flow rate was regulated during tests. Drawing of cavitating venturi is shown in Figure 3.

2.1. Test Motor. A motor has been designed which is flexible for different injector test, variable with length of prechamber and postchamber. A fuel grain with different length and port diameter can be tested in this motor configuration. Figure 4 shows a schematic of designed motor.

A prechamber is considered at the inlet of the combustion chamber, to make sure of complete evaporation of liquid oxidizer before reaching the fuel surface. Postchamber is considered to complete the combustion of unburned fuel vapor at the end of the fuel grain. The length of postchamber has a significant effect on combustion efficiency [17].

Injectors are used to atomize and vaporize oxidizer before reaching fuel grain. Injectors with 1-, 1.5-, and 2-millimeter orifice diameters were used for axial injection tests. For swirl flow tests, a new injector head flange was designed with four tangential injector slots and one axial injector slot as shown in Figure 5.

2.2. Test Procedure. Five tests were conducted based on test design. Four tangential injection tests and one axial injection test were conducted. The axial injection test which is called the benchmark test is representing a series of tests which have been conducted with the axial injection configuration. The oxidizer mass flux was changed in swirl flow tests in order to study the regression change with it.

To conduct a test, nitrous oxide is fed to the run tank from reservoir tanks. High pressure air is used to pressurize nitrous oxide in the run tank. By pushing the fire button, the oxidizer valve opens and oxidizer injects to the motor. After 0.5 seconds, igniter is triggered and combustion starts. After test time, which is usually set to 5 seconds, oxidizer valve will close and purge line will open. There is a bypass line to an environment which opens as well. This line helps to terminate thrust instantly and to have a sharp pressure and thrust profile at the end of the test, which leads to more accurate average results.

Cavitating venturi is used for maintaining the oxidizer mass flow rate. Cavitating venturi regulates the flow rate while downstream pressure fluctuates or changes. Experiments show that cavitating venturi can withstand downstream pressure changes up to 85 percent of upstream pressure and delivers almost constant mass flow rate [18]. Although there would be two-phase flow at cavitating venturi throat, oxidizer changes to liquid immediately after venturi and it can be ensured that oxidizer enters the motor in liquid form as there is a far distance between venturi and motor.

2.3. Data Reduction. In order to study the performance of motors, pressure before nozzle, igniter pressure, injection pressure, thrust, fuel mass variation, and the oxidizer flow rate were measured. Using these data, ballistic parameters of the motor, such as fuel regression rate, combustion efficiency, and specific impulse, were derived.

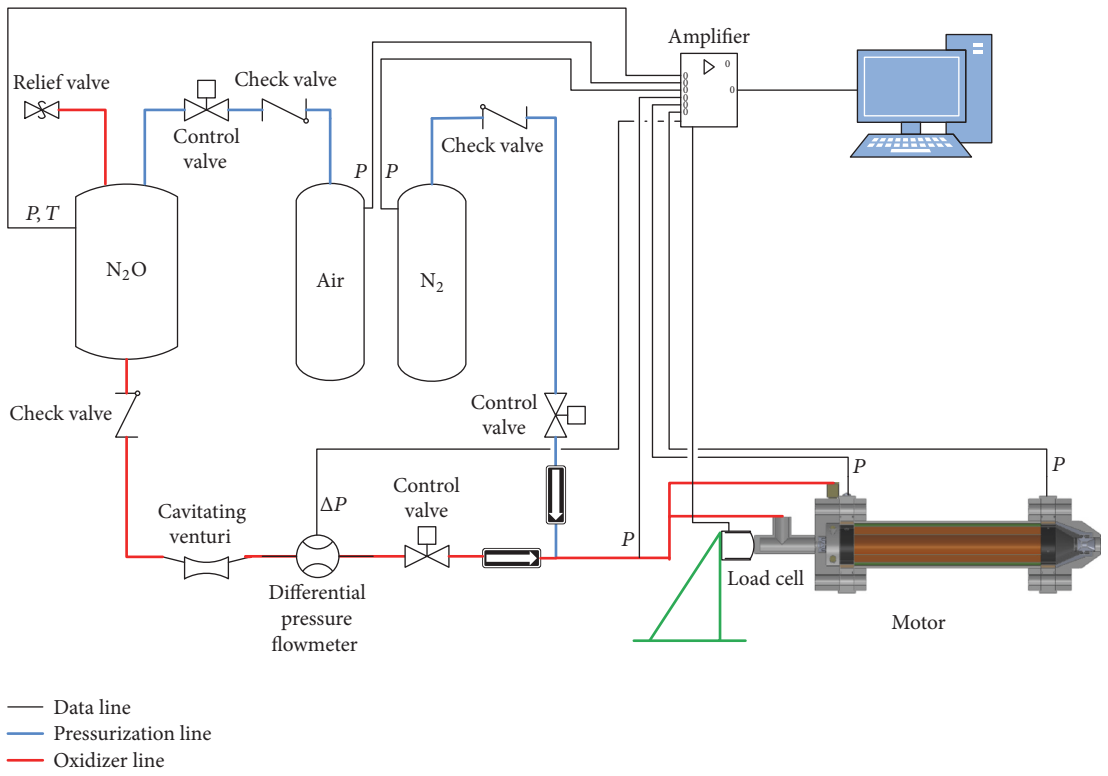

Figure 2: Schematic of the hybrid rocket motor system.

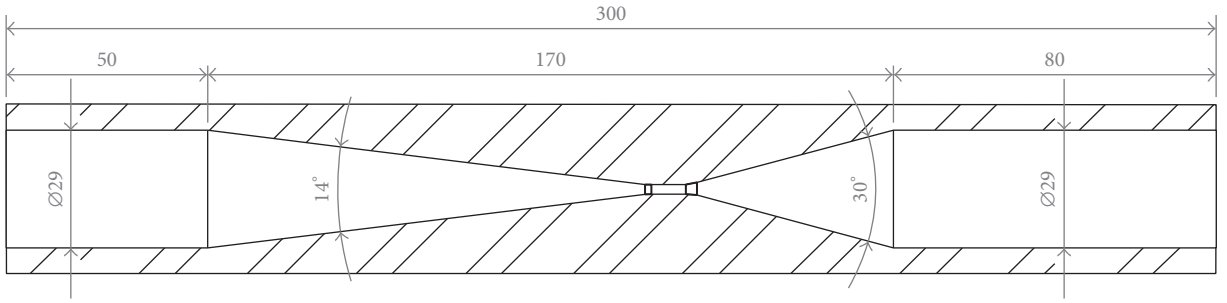

Figure 3: Cavitating venturi drawing.

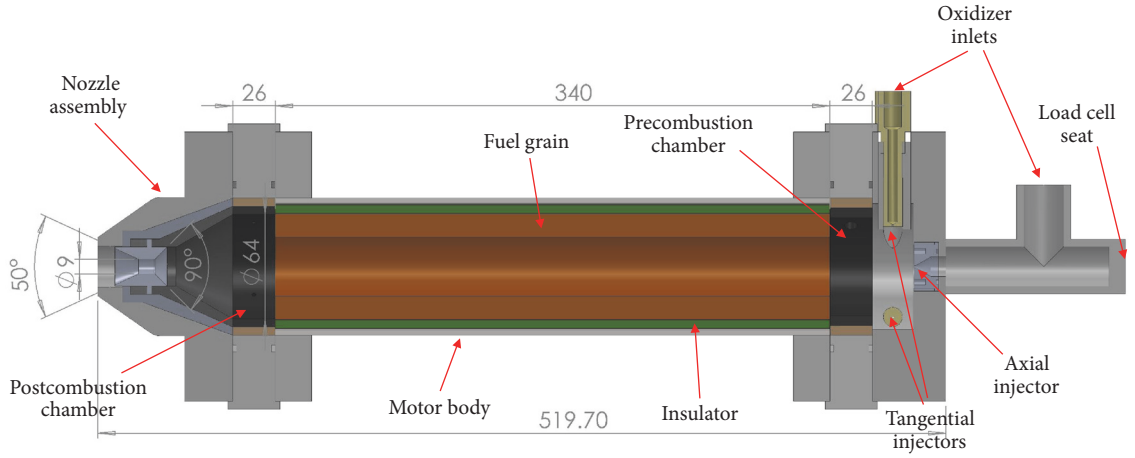

Figure 4: Subscale test hybrid motor.

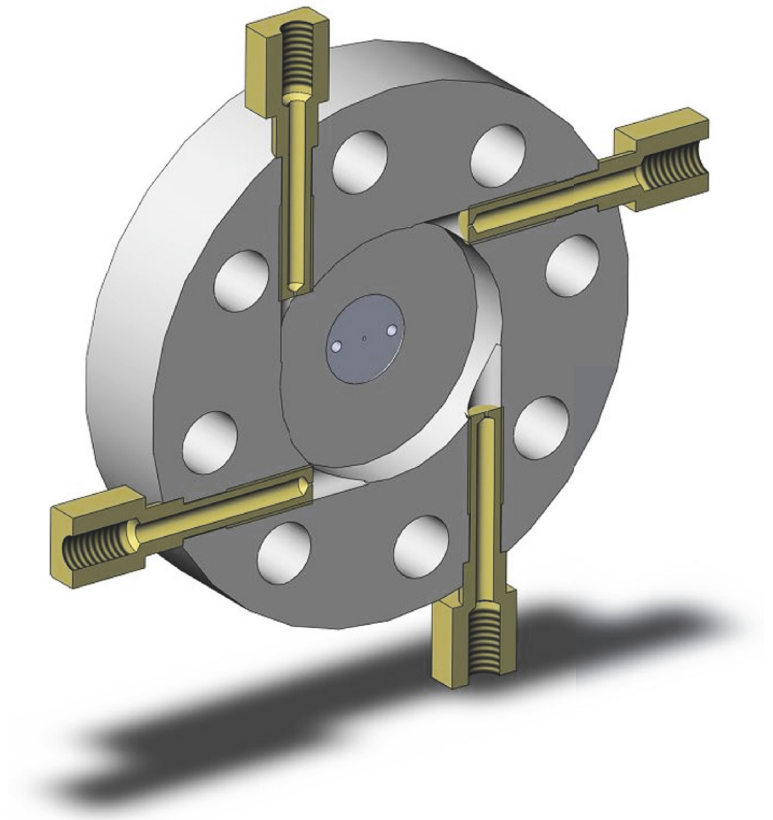

Figure 5: Section view of tangential injection cap.

Regression Rate. The average spatial and temporal regression rate can be evaluated by

$$\bar{\dot{r}} \cong \frac{\overline{D_f} - D_i}{2t_b}. \tag{1}$$

In (1), D_i is initial grain port diameter, which is measured before the test, t_b is burning time, and $\overline{D_f}$ is average final grain port diameter. Burning time is defined as the time between ignition and thrust termination. As the setup is designed in a way to have fast thrust termination, the calculated average regression rate would be accurate. The final port diameter is usually nonuniform along fuel grain; hence, the average final port diameter will be estimated with an equivalent average final diameter by

$$\overline{D_f} = \sqrt{\frac{4\left(m_{\text{fuel}_i} - m_{\text{fuel}_f}\right)}{\pi\rho_{\text{fuel}}L} + D_i^2}. \tag{2}$$

In (2) m_{fuel_i} and m_{fuel_f} are initial and final fuel grain masses, respectively. The fuel density is defined by ρ_{fuel} which is 930 kg/m^3 and L is the fuel grain length.

The calculated regression rate for the swirling oxidizer flow was compared with axial oxidizer flow regression rate. Classical relation to hybrid solid-fuel regression rate, introduced by Chiaverini [19], is

$$\dot{r} = aG_{\text{ox}}^n. \tag{3}$$

In this relation a and n are empirical constants and G_{ox}^n is oxidizer mass flux passing through the fuel grain port which will be discussed later.

Oxidizer Mass Flow Rate and Mass Flux. The mass flow rate ($\dot{m}_{\text{ox}}$) of a cavitating venturi is calculated by

$$\dot{m} = C_d A_{\text{th}} \sqrt{2\rho\left(P_{\text{up}} - P_{\text{th}}\right)}. \tag{4}$$

In (4), C_d, A_{th}, and P_{th} are venturi discharge coefficient, throat area, and throat pressure, respectively, ρ being oxidizer density, and P_{up} is upstream pressure. Cavitating venturi has been designed such that throat pressure is less than the vapor pressure of fluid at working temperature. Therefore, P_{th} will be vapor pressure of oxidizer. For venturies with converging angle more than 10° the discharge coefficient is above 99 percent as shown by Reader-Harris et al. [20]. The converging angle of venturi in this study was 30° as shown in Figure 3. Therefore, the discharge coefficient in venturi formula has been neglected.

Oxidizer mass flux determines the regression rate of the fuel grain. As the regression rate is measured with time and space average during burn time, it is convenient to measure oxidizer mass flux the same way. Average oxidizer mass flux is calculated by

$$\overline{G}_{\text{ox}} \cong \frac{\dot{m}_{\text{ox}}}{\overline{A}_p}. \tag{5}$$

In (5), $\dot{m}_{ox}$ is oxidizer mass flow rate and $\overline{A}_p$ is average port area and it is estimated by following equation:

$$\overline{A}_p = \frac{\pi D_{avg}^2}{4}. \quad (6)$$

Here, D_{avg} is average port diameter that is average of initial and final port diameter. Substituting (6) and average port diameter in (5) yields (7), which can be measured by test instruments.

$$\overline{G}_{ox} = \frac{16\dot{m}_{ox}}{\pi\left(\overline{D_f} + D_i\right)^2}. \quad (7)$$

Combustion Efficiency. Combustion efficiency of the motor will be obtained by dividing the characteristics velocity of the test to theoretic ideal characteristics velocity.

$$\eta_{combustion} = \frac{C^*_{exp}}{C^*_{theory}}. \quad (8)$$

Characteristics velocity indicates the energy released by combustion of propellant composition. The theoretic ideal characteristics velocity is calculated by a chemical equilibrium code like CEA [21]. Characteristics velocity of tests has been calculated as below.

$$C^*_{exp} = \frac{\overline{P_c} A_{th}}{\dot{m}_{nozz}}. \quad (9)$$

In (9), P_c is the average combustion chamber pressure, A_{th} is nozzle throat area, and $\dot{m}_{nozz}$ is the average mass flow rate through nozzle which is approximated by oxidizer mass flow rate and average fuel mass flow rate.

2.4. Error Analysis. Some of the variables such as regression rate, thrust, and oxidizer mass flux were reduced from test data. In order to quantify the uncertainty of these variables, an error analysis has been performed for them. The first variable to be analyzed is the final port diameter, which is calculated by (2). The relative error of the final diameter consists of the relative errors in the measurement of change in fuel grain mass, fuel density, and fuel grain length and can be estimated by (10).

$$E_{D_f} = \sqrt{\left(\frac{D_i}{D_f} E_{D_i}\right)^2 + \left(\frac{1}{2}\frac{D_f - D_i}{D_f}\right)^2 \left(E_{\Delta M}{}^2 + E_{\rho_{fuel}}{}^2 + E_L{}^2\right)}. \quad (10)$$

Next variable which is reduced from test data is the regression rate, which is calculated by (1). Based on this equation, the relative error of regression rate can be calculated using the following expression:

$$E_r = \sqrt{\left(\frac{D_f}{D_f - D_i} E_{D_f}\right)^2 + \left(\frac{1}{D_f - D_i} E_{D_i}\right)^2 + E_t{}^2}. \quad (11)$$

Table 1: Relative errors of test variables.

Variable	Relative error
D_i	0.004
ΔM	0.0001
ρ_{fuel}	0.0107
L	0.0004
t	0.002
D_t	0.01
T_{ox}	0.0071
ΔP	0.0001
D_f	0.0034
r	0.0208
$\dot{m}_{ox}$	0.0203
$\overline{G}_{ox}$	0.0209

Oxidizer mass flux is a function of oxidizer mass flow rate and initial and final diameter, as (7). Therefore, the relative error of this variable can be evaluated as follows:

$$E_{\overline{G}_{ox}} = \sqrt{\left(\frac{2D_f}{D_f + D_i} E_{D_f}\right)^2 + \left(\frac{2D_i}{D_f + D_i} E_{D_i}\right)^2 + E_{\dot{m}_{ox}}{}^2}. \quad (12)$$

The relative error of oxidizer mass flow rate itself consists of relative error of feed pressure, diameter of cavitating venturi nozzle, and oxidizer temperature, based on (4).

$$E_{\dot{m}_{ox}} = \sqrt{\left(2E_{D_t}\right)^2 + \left(\frac{1}{2}E_{T_{ox}}\right)^2 + \left(\frac{1}{2}E_{\Delta P}\right)^2}. \quad (13)$$

The relative errors for one of the tests have been calculated and are presented in Table 1.

3. Test Results and Discussion

Before swirl flow tests, a series of tests had been conducted using a single oxidizer axial injector. The fuel regression rate for axial oxidizer injection had been derived by using these tests. One of these tests has been reported as a benchmark for comparison between the swirl flow test results with axial flow test results. Ballistic characteristics of axial flow tests are presented in Table 2.

The experimental regression rate of axial flow tests with the same fuel and oxidizer combination as this study had been reported as

$$\dot{r} = 0.40 G_{ox}^{0.37}. \quad (14)$$

Motor configurations for tests conducted in this study are presented in Table 3.

The two first vortex flow tests were performed with one axial injector's and four tangential injectors' configuration. Pressure and thrust profiles of these tests are shown in Figures 6 and 7.

The third test was done by using the four tangential injectors' and one axial injector's configuration. The fuel

Table 2: Ballistic characteristics of axial flow tests.

Test #	t_{burn} (sec)	$P_{chamber}$ (bar)	T_{motor} (kgf)	m_f (g/s)	D_{final} (mm)	O/F	C^*_{exp} (m/sec)	η_{c^*}
1-S0A1	7.60	39.2	43.2	53	54.81	3.23	1302.59	0.89
2-S0A1	9.00	37.5	41.3	51	55.11	3.54	1236.80	0.81
3-S0A1	7.43	36.7	40.72	48	53.24	3.54	1328.86	0.89
4-S0A1	7.54	34.47	38.53	41	41.82	4.26	1307.77	0.84
5-S0A1	7.72	24.29	38.55	41	38.36	4.42	1210.54	0.77

Table 3: Motor configurations for tests.

	Axial injector number	Tangential injector number	Precombustion chamber	Postcombustion chamber
0-bench	1	0	Yes	No
1-S4A1	1	4	Yes	No
2-S4A1	1	4	Yes	No
3-S4A1	1	4	No	Yes
4-S4A1	1	4	Yes	No

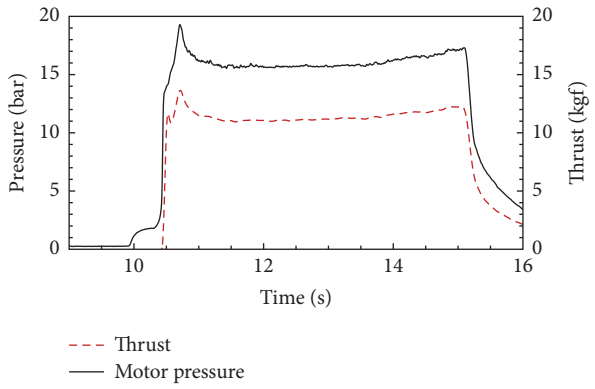

Figure 6: Pressure and thrust profile of test #1.

grain was pushed toward the nozzle entrance, according to Figure 4, to provide a larger precombustion chamber and to give more time for evaporating the oxidizer. It was expected to have more uniform fuel grain surface after test, compared to test with axial injector. Pressure and thrust versus time are shown in Figure 8.

The fourth test was done by the same injector configuration as test #3. Precombustion chamber configuration was changed to its initial state, that is, as tests #1 and #2. Postcombustion chamber was used in its original place at the aft end of the motor, before nozzle entrance. The pressure and thrust profiles of this test are shown in Figure 9.

Specifications of swirl flow tests and axial flow test are shown in Table 4.

The oxidizer mass flow rate either could be calculated by (4) and using test data or could be measured by a differential pressure flow meter used in oxidizer feed line. Results are shown in Table 5.

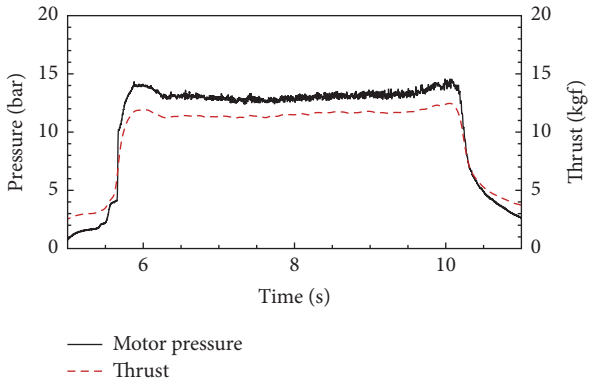

Figure 7: Pressure and thrust profile of test #2.

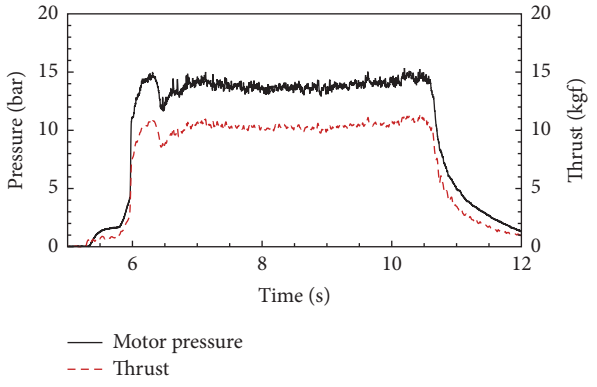

Figure 8: Pressure and thrust profile of test #3.

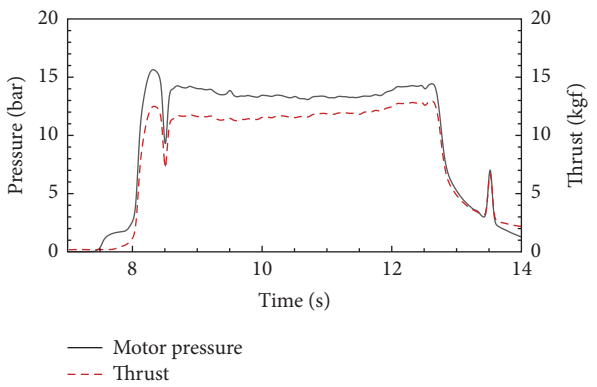

Figure 9: Pressure and thrust profile of test #4.

Table 4: Specification of tests.

Test #	Motor specs		Fuel specs (before test)		Injector specs		
	D_{th} (mm)	D_i (mm)	L_{grain} (mm)	m_{fuel_i} (g)	Axial injector number	Tangential injector number	$D_{injector}$ (mm)
0-bench	9.0	49.0	251	706.4	1	0	1.5
1-S4A1	9.1	42.0	249	856.8	1	4	1.0
2-S4A1	9.1	45.5	248	660.0	1	4	1.0
3-S4A1	9.1	48.8	240	623.8	1	4	1.0
4-S4A1	9.1	43.3	248	846.0	1	4	1.0

Table 5: Oxidizer mass flow rate.

Test #	T_{N_2O} (°C)	ρ_{N_2O} (kg/m^3)	P_{sat} (bar)	P_{up} (bar)	m_{ox} (g/s)
1-S4A1	25.0	743.9	56.6	69.7	60.0
2-S4A1	26.8	708.3	57.6	70.0	56.5
3-S4A1	25.8	721.7	56.3	69.2	59.7
4-S4A1	26.5	712.4	57.2	68.7	55.1

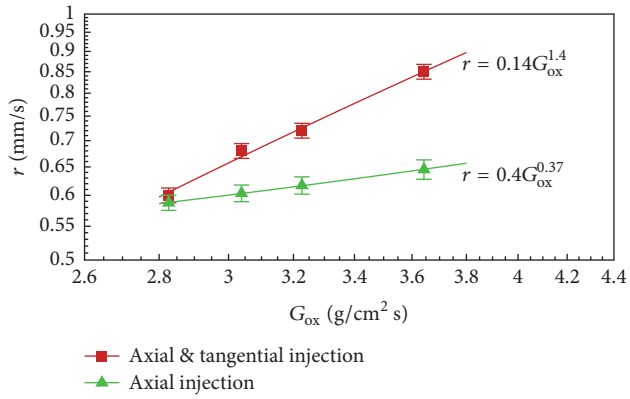

Figure 10: Fuel regression rate versus oxidizer mass flux.

Motor performance and ballistic analysis have been done for tests. The results of these calculations are provided in Table 6, as well.

Test results show that although oxidizer mass flux in benchmark test is higher than swirl flow tests, the fuel regression rate is lower compared to swirl flow tests. By comparing these values with results of bulk regression rate, which derived from swirl tests, the results show enhancement of regression rate is due to tangential injection in the combustion chamber. Figure 10 shows the fuel regression rate versus oxidizer mass flux for swirling oxidizer flow and axial oxidizer flow.

The fuel regression rate for a combination of axial and tangential oxidizer injection has been derived and the relation is

$$\dot{r} = 0.14 G_{ox}^{1.40}. \quad (15)$$

The difference between the regression rate exponent of swirl flow and axial flow motors can be explained as follows. Classical solid-fuel regression rate relation in hybrid motors is derived by relating heat transfer at the fuel surface to the momentum of the flow. This is done by boundary layer analogies such as Reynolds analogy or Chilton-Colborn analogy. Axial momentum or mass flux is being used in classical hybrid relation, whereas, in a swirl flow motor, there is a tangential mass flux and momentum which is not taken into account.

There are two reasons for explanation of increase in the fuel regression rate. First, centrifugal force caused by swirl flow compresses reacting boundary layer which increases heat feedback to the fuel surface and increases the fuel pyrolysis rate. Second, the convection heat coefficient will be enhanced by swirling the flow, which increases heat flux to the fuel grain. It has been shown numerically that velocity magnitude in the flow field increases when flow is swirled [15]. This results in increase in heat transfer at the fuel surface which increases the regression rate as a consequence.

3.1. Effect of Swirl Flow. The equivalent regression rate is introduced in order to better compare fuel regression rate between two types of flows. The test regression rate is assumed to consist of two parts as shown in

$$\dot{r}_{test} = \dot{r}_{equivalent} + \dot{r}_{tang}. \quad (16)$$

Part one is the contribution of axial flow and part two is the contribution of swirl flow. By using (14), equivalent fuel regression rate of the swirl flow tests mass fluxes has been calculated. The results are shown in Table 7.

It could be seen from Table 7 that, by applying the tangential injection, the regression rate of fuel grain has been improved. It was shown in Figure 11 that the increasing tangential mass flux of oxidizer will increase the regression rate contribution due to swirl flow.

According to Table 6, oxidizer-to-fuel ratio of benchmark test was more than swirl flow tests. This results in higher characteristics velocity. Variation of characteristics velocity with respect to oxidizer-to-fuel ratio for tests pressures is shown in Figure 12. Experimental characteristics velocity has been derived and is shown in Figure 12, too.

The propellant used in this study has an optimum O/F of around 6.5. Both axial flow and swirl flow tests had O/F ratios far enough from this value. Therefore, low O/F effect applies to both cases, where it is easier to achieve higher efficiency comparing to optimal O/F.

Table 6: Ballistic characteristics of tests.

Test #	t_{burn} (sec)	$P_{chamber}$ (bar)	T_{motor} (kgf)	m_f (g/s)	D_{final} (mm)	r_f (mm/s)	O/F	G_{ox} (g/cm^2 s)	C^*_{exp} (m/sec)	η_{c^*}
0-bench	6.59	24.90	21.39	22	58.20	0.56	3.88	3.829	1288.32	0.88
1-S4A1	4.48	15.60	12.06	28	49.61	0.85	2.12	3.643	1213.57	0.99
2-S4A1	4.66	12.83	11.30	24	51.83	0.68	2.36	3.039	1108.53	0.91
3-S4A1	5.04	12.96	11.11	22	54.66	0.60	2.72	2.840	1102.85	0.87
4-S4A1	4.62	13.43	11.55	25	49.96	0.72	2.25	3.228	1168.69	0.97

Table 7: Regression rate changes due to swirl flow.

Test #	$r_{equivalent}$ (mm/s)	r_{test} (mm/s)	Δr (%)
1-S4A1	0.64	0.85	33.00
2-S4A1	0.60	0.67	13.56
3-S4A1	0.58	0.60	3.80
4-S4A1	0.61	0.72	18.33

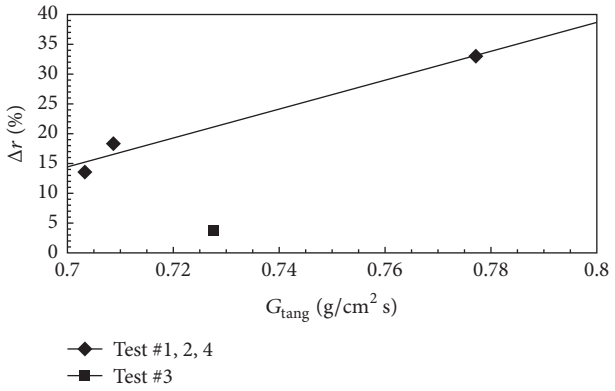

Figure 11: Effect of swirl flow on regression rate.

It is clear that characteristics velocity is improved by swirl flow. Combustion efficiency or characteristics velocity efficiency has been calculated by dividing experimental characteristics velocity by theoretical characteristics velocity for each test with specific test conditions. Based on these results, it is clear that combustion efficiency of swirl tests was higher than benchmark test. Furthermore, it has been shown that, by removing postcombustion chamber in test #3, combustion efficiency was reduced compared to other swirl flow tests. Combustion efficiency of tests has been plotted in Figure 13 to show the effect of tangential oxidizer injection on the combustion performance of the motor. Axial injection efficiencies relate to tests which relation 14 has been derived from.

Figure 13 shows that, by applying tangential oxidizer injection, combustion efficiency increased by almost 10%. This improvement is mainly due to better mixing between the oxidizer and pyrolysed fuel. This will reduce the time needed for reactants to be consumed. In addition, reactants travel a longer path before they exit from the motor nozzle, when swirl flow is applied. Consequently, they have more time to react or to complete the reaction. Combustion efficiency will be improved in this way.

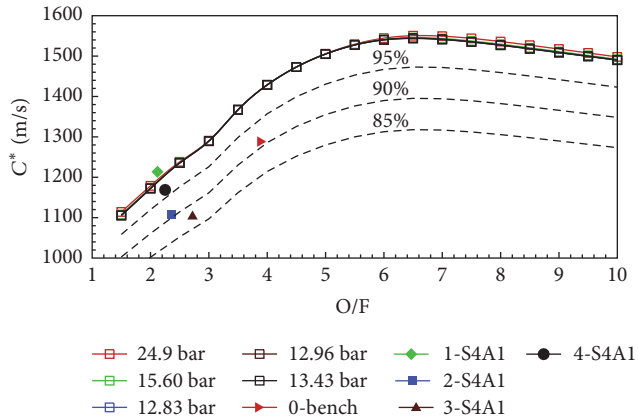

Figure 12: Effect of swirl flow on characteristics velocity.

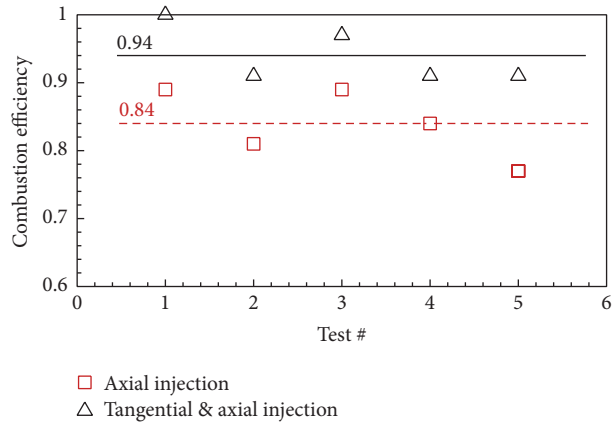

Figure 13: Comparison of combustion efficiency for oxidizer swirl flow and axial flow.

The discharge coefficient of the nozzle may be reduced due to swirl flow. This effect will increase the motor pressure. As characteristics velocity is only a function of propellant characteristics and combustion chamber properties, the nozzle behavior does not affect this variable directly. Also, checking the effect of chamber pressure on characteristics velocity shows it is negligible as shown in Figure 12. Therefore, swirl flow will not affect the combustion efficiency of motor by reducing discharge area of nozzle.

3.2. Effect of Pre- and Postcombustion Chamber. The square symbol point in Figure 11 is related to the regression rate of

test #3, which had a longer precombustion chamber. Liquid N_2O atomizes and vaporizes as it enters the combustion chamber. This process needs a duration time or delay time to be completed. On the other hand, because the chemical reaction type of hybrid motor is gas phase combustion, the oxidizer should be vaporized before entering to the flame zone and reacting with fuel vapor. By applying tangential injection, oxidizer flow path will be extended before it reaches the fuel grain. This will help to have good mixing between the oxidizer and fuel from the lead of fuel grain and to have a uniform fuel grain surface after the test. Therefore, for comparison between swirl flow tests, the third test was done to see if giving more time to liquid oxidizer for vaporizing helps to improve motor performance and to have a more uniform fuel grain surface after the test.

Test results show that lengthening precombustion chamber not only did not improve the regression rate but also decreased the effect of swirl flow, although more study is needed to see if there is an optimum value for precombustion chamber length.

It was mentioned before that, for test #3, postcombustion chamber was shorter than other tests. It can be seen in Figures 12 and 13 that shorter postcombustion chamber results in lower combustion efficiency. The reason is shorter postcombustion chamber is equivalent to lower characteristics velocity (L^*) which is a well-known criterion for combustion efficiency.

3.3. Effect of Chamber Pressure. By looking at Table 6, one can conclude that pressure does not have a distinctive effect on regression rate or combustion efficiency. Test #3 cannot be compared with other tests as it has a different condition.

4. Conclusion

In this study, the swirling oxidizer flow effects on the fuel regression rate and motor performance of a HTPB/N_2O hybrid rocket motor have been investigated. A laboratory setup and a modular motor were developed and were fabricated. The motor and laboratory were designed to have a full control of parameters such as oxidizer mass flow rate, number and configuration of injectors, and pre- and postchambers, for further investigations. Swirl flow tests were conducted with one axial and four tangential injectors. Several conclusions are listed as follows:

(1) The fuel regression rate for swirl oxidizer flow tests was estimated by average spatial and temporal method and has been compared with axial oxidizer flow tests. Results show enhancement in the fuel regression rate.

(2) It was seen that fuel regression rate relation, derived from swirl flow tests, has different coefficient values compared to classical hybrid fuel regression rate relations. This indicates a different reacting boundary layer structure.

(3) It was shown that regression rate enhancement can be related to tangential oxidizer mass flux.

(4) Results of swirl flow tests show that, by applying swirling oxidizer flow, overall combustion efficiency increased almost by 10% and nearly complete combustion was achieved. This shows a better mixing between the oxidizer and fuel in the combustion chamber.

(5) Although combustion efficiency was increased by swirling the oxidizer flow, removing postcombustion chamber decreased the combustion efficiency. This confirms the need to use postcombustion chamber even in the swirl flow motor.

(6) It was shown that providing more length in the precombustion chamber does not improve the performance of the motor or the regression rate of the fuel grain. This indicates that liquid nitrous oxide had sufficient time to vaporize completely before reaching fuel grain in original motor design. Besides, larger length of the precombustion chamber leads to weaker swirl flow which is not desirable.

Conflicts of Interest

The authors declare that they have no conflicts of interest.

References

[1] J. P. de la Beaujardiere, M. Brooks, S. Chowdhury, B. Genevieve, and L. Roberts, "The phoenix hybrid sounding rocket program: a progress report," in *Proceedings of the 17th AIAA International Space Planes and Hypersonic Systems and Technologies Conference*, San Diego, California, CA, USA, 2011.

[2] L. Casalino and D. Pastrone, "Optimization of hybrid sounding rockets for hypersonic testing," *Journal of Propulsion and Power*, vol. 28, no. 2, pp. 405–411, 2012.

[3] J. Lieh, E. Spahr, A. Behbahani, and J. Hoying, "Design of hybrid propulsion systems for unmanned aerial vehicles," in *Proceedings of the 17th AIAA International Space Planes and Hypersonic Systems and Technologies Conference*, San Diego, California, CA, USA, 2011.

[4] A. Mack and J. Steelant, "FAST20XX: First progress on European future high-altitude high-speed transport," in *Proceedings of the 17th AIAA International Space Planes and Hypersonic Systems and Technologies Conference 2011*, April 2011.

[5] G. Cai, H. Zhu, D. Rao, and H. Tian, "Optimal design of hybrid rocket motor powered vehicle for suborbital flight," *Aerospace Science and Technology*, vol. 25, no. 1, pp. 114–124, 2013.

[6] M. Ambrogio, "The FP7 SPARTAN Program Status and Achievements," in *Space Propulsion*, Bordeaux, France, 2012.

[7] A. Karabeyoglu, J. Stevens, D. Geyzel, B. Cantwell, and D. Micheletti, "High performance hybrid upper stage motor," in *Proceedings of the 47th AIAA/ASME/SAE/ASEE Joint Propulsion Conference and Exhibit 2011*, San Diego, CA, USA, August 2011.

[8] C. C. Jones, D. D. Myre, and J. S. Cowart, "Performance and analysis of vortex oxidizer injection in a hybrid rocket motor," in *Proceedings of the 45th AIAA/ASME/SAE/ASEE Joint Propulsion Conference and Exhibit*, Denver, Colorado, CO, USA, August 2009.

[9] M. Masugi, T. Ide, S. Yuasa, T. Sakurai, N. Shraishi, and A. T. Shimad, "Visualization of Flames in Combustion Chamber of

Swirling-Oxidizer-Flow-Type Hybrid Rocket Engines," in *Proceedings of the in 46th AIAA/ASME/SAE/ASEE Joint Propulsion Conference Exhibit*, Nashville, Tennessee, TN, USA, 2010.

[10] N. Bellomo, F. Barato, M. Faenza, M. Lazzarin, A. Bettella, and D. Pavarin, "Numerical and experimental investigation on vortex injection in hybrid rocket motors," in *Proceedings of the 47th AIAA/ASME/SAE/ASEE Joint Propulsion Conference and Exhibit 2011*, San Diego, California, Ca, USA, August 2011.

[11] S. Yuasa, K. Yamamoto, H. Hachiya, K. Kitagawa, and Y. Oowada, "Development of a small sounding hybrid rocket with a swirling-oxidizer-type engine," in *Proceedings of the 37th Joint Propulsion Conference and Exhibit*, AIAA 2001-3537, AIAA, Salt Lake City, Utah, UT, USA, July 2001.

[12] S. Yuasa, O. Shimada, T. Imamura, T. Tamura, and K. Yamamoto, "A technjque for improving the performance of hybrid rocket engines," in *Proceedings of the in 35th AIAA/ASME/SAE/ASEE Joint Propulsion Conference Exhibit*, Los Angeles, California, CA, USA, 1999.

[13] T. Tamura, S. Yuasa, and K. Yamamoto, "Effects of Swirling Oxidizer Flow on Fuel Regression Rate of Hybrid Rockets," in *Proceedings of the in 35th AIAA/ASME/SAE/ASEE Joint Propulsion Conference Exhibit*, Los Angeles, 1999.

[14] W. H. Knuth, M. J. Chiaverini, J. A. Sauer, and D. J. Gramer, "Solid-fuel regression rate behavior of vortex hybrid rocket engines," *Journal of Propulsion and Power*, vol. 18, no. 3, pp. 600–609, 2002.

[15] C. P. Kumar and A. Kumar, "Effect of swirl on the regression rate in hybrid rocket motors," *Aerospace Science and Technology*, vol. 29, no. 1, pp. 92–99, 2013.

[16] M. Byko, "SpaceShipOne, the Ansari X Prize, and the materials of the civilian space race," *Feature Materials World*, vol. 56, no. 11, pp. 24–28, 2004.

[17] M. Chiaverini, "Fundamental of hybrid rocket combustion and propulsion," in *Proceedings of the Chemical Engineering Progress Symposium Series*, vol. 62, 1966.

[18] H. Ghassemi and H. F. Fasih, "Application of small size cavitating venturi as flow controller and flow meter," *Flow Measurement and Instrumentation*, vol. 22, no. 5, pp. 406–412, 2011.

[19] M. Chiaverini, "Review of solid-fuel regression rate behavior in classical and nonclassical hybrid rocket motors," in *Fundamentals of Hybrid Rocket Combustion and Propulsion*, pp. 37–126, American Institute of Aeronautics and Astronautics, Virginia, VA, USA, 2006.

[20] M. J. Reader-Harris, W. C. Brunton, J. J. Gibson, D. Hodges, and I. G. Nicholson, "Discharge coefficients of venturi tubes with standard and non-standard convergent angles," *Flow Measurement and Instrumentation*, vol. 12, no. 2, pp. 135–145, 2001.

[21] B. J. McBride and S. Gordon, *Computer Program for Calculation of Complex Chemical Equilibrium Compositions and Applications*, NASA Reference Publications, Ohio, OH, USA, 1994.